

Local bias-induced phase transitions

Electrical bias-induced phase transitions underpin a wide range of applications from data storage to energy generation and conversion. The mechanisms behind these transitions are often quite complex and in many cases are extremely sensitive to local defects that act as centers for local transformations or pinning. Using ferroelectrics as an example, we review methods for probing bias-induced phase transitions and discuss the current limitations and challenges for extending the methods to field-induced phase transitions and electrochemical reactions in energy storage, biological and molecular systems.

Sergei V. Kalinin¹, Brian J. Rodriguez², Stephen Jesse, Peter Maksymovych, Katyayani Seal, Maxim Nikiforov, and Arthur P. Baddorf
The Center for Nanophase Materials Sciences, Oak Ridge National Laboratory, Oak Ridge, TN 37922, USA

Andrei L. Kholkin

Department of Ceramics and Glass Engineering, CICECO, University of Aveiro, 3810-193 Aveiro, Portugal

Roger Proksch

Asylum Research, Santa Barbara, CA 93117, USA

¹ E-mail: sergei2@ornl.gov

² Present address: *Max Planck Institute of Microstructure Physics, Weinberg 2, D-06120 Halle, Germany.*

Bias-induced phase transitions in functional materials

The operation of the multitude of electrical, electronic and energy storage devices that underpin modern civilization is universally based on the interactions between electrical bias and matter. Multiple examples in energy technologies include electrochemical reactions in fuel cells, photoelectrochemical cells and batteries. The need for technology to replace Complementary Metal–Oxide–Semiconductor (CMOS) devices (see <http://www.ITRS.net>) has stimulated the search for alternative data-storage and information-processing mechanisms, ranging from spin–electron coupling in Magnetic Random Access Memory

(MRAM) devices (see <http://www.ITRS.net>), to electron–lattice coupling in ferroelectric RAM^{1,2} and data storage³, to electrically triggered phase transitions in Phase Change Memory (PCM) devices⁴. The operation of molecular self-assembled monolayer-based memory devices⁵ is often derived from the growth and dissolution of conductive metal filaments, giving rise to the concept of 'Electrochemical Memory' (EM)⁶. In many of these cases, the operational principle of the device is directly founded on a bias-induced phase or electrochemical transformation, be it polarization switching in ferroelectrics, amorphization and crystallization in PCM, or reversible electrochemical reactions in EM.

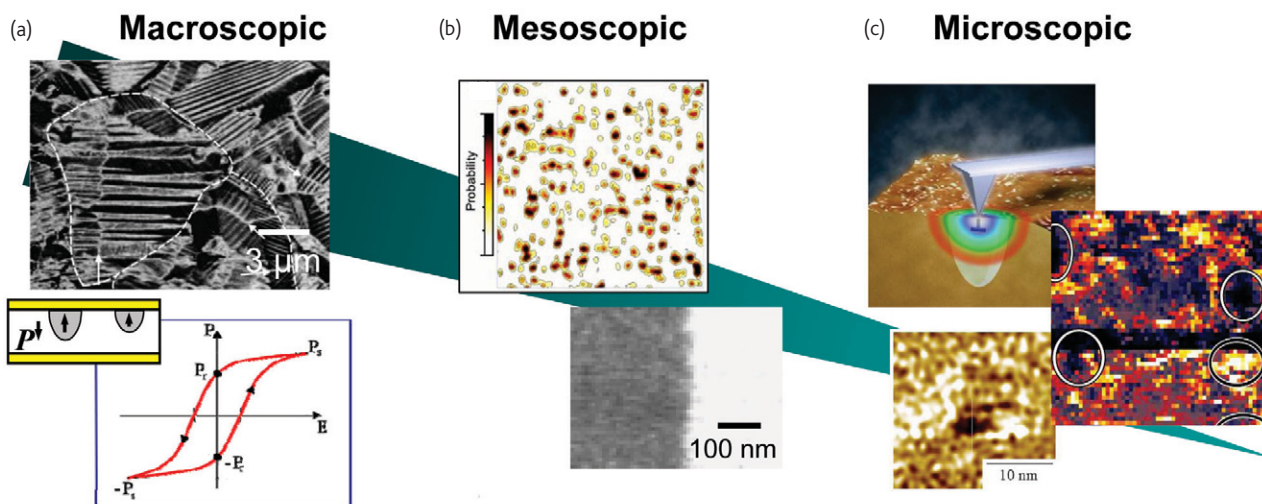


Fig. 1 Polarization dynamics in ferroelectrics from the macro- to microscopic scales. (a) Macroscopic scale: bulk ceramics (reproduced with permission from Lupascu and Rabe¹⁰⁸) and polarization-electric field loops in macroscopic capacitors. (b) Spatial probability of nucleation sites in a $6 \times 6 \mu\text{m}^2$ scan area of an epitaxial PZT capacitor structure (reproduced with permission from Kim *et al.*²⁰) and domain-wall roughness in epitaxial PZT (reproduced with permission from Paruch *et al.*¹³). (c) Local switching by SPM to reveal spatial variation of the switching properties (reproduced with permission from Jesse *et al.*⁷²) and to write nanometer scale domains (reproduced with permission from Tanaka *et al.*⁶⁰).

In many cases, the mechanisms behind bias-induced transitions are extremely complex and include charge and mass transport, electrochemical processes, thermal exchange and interface effects. The phase transformation fronts are often unstable and even small perturbations grow exponentially, giving rise to conductive channels in PCM, needle-like domain morphologies in ferroelectrics, or dendrite metal growth in electrochemical systems. The system is thus extremely sensitive to local defects that act as centers for local transformations. The density and energy distribution of the defects thus determine the overall performance of the material, including the kinetics and thermodynamics of bias-induced transitions, fatigue, and various related parameters.

Ferroelectric materials

Polarization reversal in ferroelectric materials is not associated with significant thermal effects, mass transport, or lattice rearrangement, and thus provides an ideal model. Like other crystalline solids, ferroelectrics contain a range of point and extended structural defects that influence local ferroelectric switching by (a) affecting local phase stability, (b) acting as sites for domain wall pinning, and (c) controlling nucleation. On the macroscopic level, defect effects on phase stability have been studied extensively using mean-field theories⁷. Similarly, the energy and spatial distribution of the nucleation sites directly control macroscopic mechanisms for polarization switching^{8–10}. However, in the macroscopic case the role of individual defects on polarization switching cannot be resolved (Fig. 1), thus limiting opportunities for materials design and optimization.

Probing the mesoscopic mechanisms for polarization switching based on domain wall morphology, domain distributions and nucleation site mapping in capacitors requires spatially resolved imaging methods

(Fig. 1). The role of defects on the domain wall motion and geometry in ferroelectric and ferromagnetic systems has been studied in detail in the context of statistical physics¹¹. Experimentally, the domain wall roughness and kinetics were addressed in a series of papers by Paruch *et al.*^{12–14}. Shvartsman and Kholkin¹⁵ and Likodimos *et al.*^{16,17} analyzed the statistical aspects of domain morphology and size distributions and provided information of the collective effect of defect centers on the switching process. Finally, recent studies by Grigoriev *et al.*¹⁸ using ultrafast focused X-ray imaging, and Gruverman *et al.*¹⁹ and Kim *et al.*²⁰ using Piezoresponse Force Microscopy (PFM) have demonstrated that in a uniform field in $\sim 100 \mu\text{m}$ capacitor structures, switching is initiated in a very small number ($\sim 1–10$) of locations and then propagates through the macroscopic (tens of micrometers) region of the film, providing information on the localization of the strong nucleation centers and the statistics of nucleation events.

Understanding the atomistic mechanisms of polarization reversal requires studies on a single (well-defined) defect level. The predominance of dislocations as the primary defect type in ferroelectric films has rendered them a natural subject. Thermodynamic modeling by Alpay *et al.*²⁴ and Balzar *et al.*²¹ have demonstrated that misfit²² and threading²³ dislocations locally destabilize the ferroelectric phase²⁴ and can thus account for a $\sim 10 \text{ nm}$ nonswitchable layer and reduced dielectric properties²⁵ in ferroelectric films. This prediction agrees with the variable-temperature electron microscopy studies by Wang *et al.*²⁶, which demonstrate a shift in the ferroelectric transition temperature in the vicinity of dislocations. Misfit dislocations aligned in the (100) and (010) directions in perovskite structures effectively couple to the 90° ferroelastic domain walls and thus serve as effective pinning centers, as studied theoretically by Pertsev²⁷ and demonstrated experimentally by Alexe *et al.*²⁸

The combination of theory and electron microscopy in many cases provides detailed information on the structural and electronic properties of individual atomic defects²⁹⁻³¹, necessitating the development of methods for probing ferroelectric functionality on the single-defect level. In this review, we summarize recent approaches for local probing of polarization dynamics in bias-induced phase transitions on mesoscopic and microscopic scales based on PFM.

Local probing of bias-induced phase transitions in ferroelectric materials

Scanning Probe Microscopy (SPM) provides a natural framework for probing local phase transitions and correlating them with microstructure. The external stimulus (either local or global) applied to the systems induces a phase transformation, while the SPM probe detects the associated change in local properties. Perhaps the best-known example is protein unfolding spectroscopy, in which the force applied by an atomic force microscope tip acts as a stimulus to change molecular conformation, and the measured change in molecule length is the response. In many cases, the unfolding is experimentally reversible³², allowing determination of the statistical distributions of the possible trajectories through the energy space of the system.

However, there are many examples of irreversible processes in SPM studies, including pressure-induced phase transitions and dislocation nucleation in nanoindentation, and thermal phase transitions, for which these approaches are inapplicable.

In PFM and Piezoresponse Force Spectroscopy (PFS), the probe concentrates an electric field in a nanoscale volume of material (with typical dimensions of ~10–50 nm) and induces local domain nucleation and growth. Simultaneously, the probe detects the onset of nucleation and the size of a developing domain via detection of the electromechanical response of the material to a small oscillatory bias. The key aspect of electromechanical detection is that it is only weakly sensitive to contact area (unlike mechanical response in SPM, where contact stiffness scales linearly with contact area), thus allowing for quantitative and reproducible measurements on rough surfaces, as discussed below.

Piezoresponse force microscopy

PFM is based on the detection of a bias-induced piezoelectric surface deformation. A conductive tip is brought into contact with a piezoelectric sample surface and the piezoelectric response of the surface is detected as the first harmonic component, $A_{1\omega}$, of the

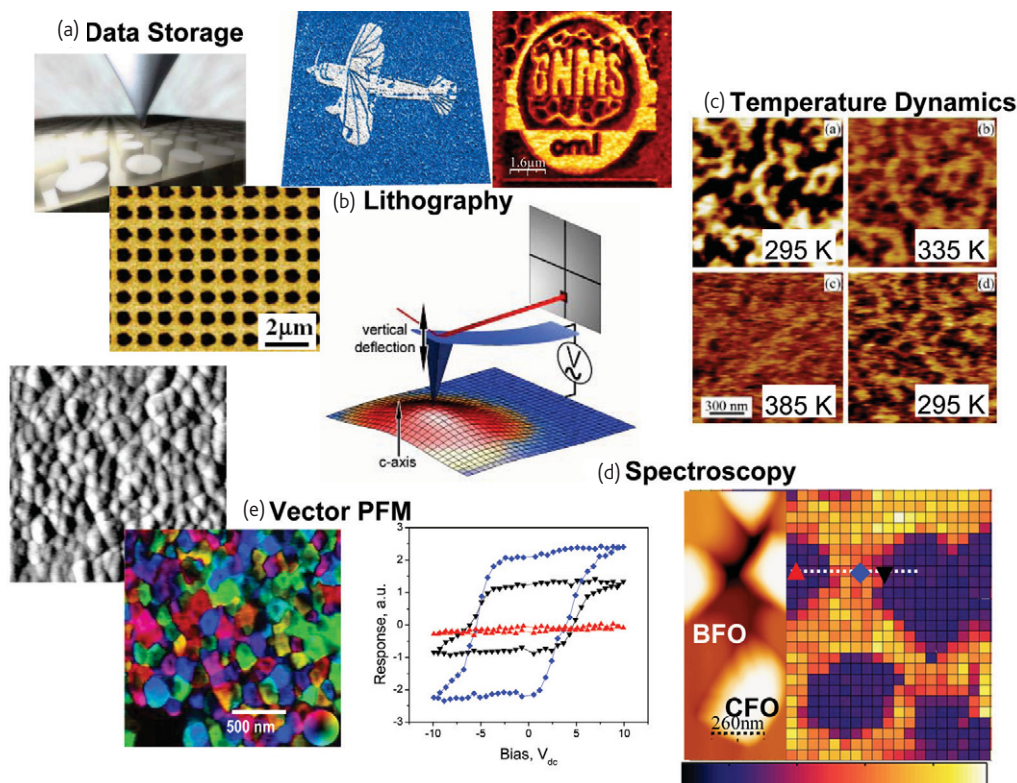


Fig. 2 The many faces of piezoresponse force microscopy. PFM can be used to investigate polarization reversal for (clockwise from the top left): (a) data-storage applications, (b) nanolithography, (c) temperature-dependent domain dynamics, (d) spectroscopy and spectroscopic mapping of switching properties. The combination of vertical and lateral PFM can be used to reconstruct the real-space polarization direction via (e) vector PFM. Data in (a) reproduced with permission from Tanaka et al.⁶⁰. Data in (c) reproduced with permission from Shvartsman and Kholkin¹⁵. (d) Adapted with permission from Rodriguez et al.⁶⁸. (e) Reproduced with permission from Kalinin et al.¹⁰⁹.

tip deflection, $A = A_0 + A_{1\omega}\cos(\omega t + \varphi)$, induced by the application of a periodic bias, $V_{\text{tip}} = V_{\text{dc}} + V_{\text{ac}}\cos(\omega t)$, to the tip (a schematic is shown in the middle of Fig. 2). The normalized deflection amplitude, $PR = A_{1\omega}/V_{\text{ac}}$ (pm/V), provides information on the magnitude of the local electromechanical coupling. The phase of the electromechanical response, φ , yields the polarization direction. The two main experimental approaches to PFM are (a) a tip-generated inhomogeneous electric field and (b) a homogeneous electric field applied via an electrical contact on top of the sample (with voltage applied externally or via the tip). In both cases, the tip serves as a probe of the local electromechanical deformation induced by the local (tip as electrode) or uniform (top electrode) field. PFM has been used to investigate a wide variety of ferroelectric phenomena ranging from vertical, lateral, and vector imaging, domain patterning and ferroelectric lithography, to variable temperature, liquid and vacuum studies, to spectroscopic imaging, as shown in Fig. 2.

The unique image formation mechanism in PFM has stimulated an extensive effort in the quantitative description of voltage-dependent contact mechanics. A rigorous solution of piezoelectric indentation is available only for the case of transversally isotropic materials³³⁻³⁵. These analyses have shown that under conditions of good electrical

contact the PFM signal is insensitive to the contact radius. This renders the measurements quantitative and only weakly sensitive to topographic cross-talk (i.e. coupling between observed signal and variations in surface topography). A general approach to calculating the electromechanical response in PFM is based on the decoupling approximation^{36,37}. In this case: (a) the electric field in the material is calculated using a rigid electrostatic model (no piezoelectric coupling, $d_{ijk} = e_{ijk} = 0$); (b) the strain or stress field is calculated using constitutive relations for a piezoelectric material, $X_{ij} = E_k e_{kij}$; and (c) the displacement field is evaluated using the appropriate Green's function for an isotropic or anisotropic solid. The decoupled theory has been applied to systematically describe the image formation mechanism in PFM including resolution and wall profiles³⁸, anisotropic material^{39,40}, finite size effects^{41,42} and spectroscopy data deconvolution⁴³.

Domain studies—growth and relaxation

PFM offers a direct pathway to probe domain switching behavior and mesoscopic structure of the domain wall in ferroelectrics. In switching studies, a DC bias pulse is applied to a static tip to create a domain, which is subsequently imaged in scanning mode. This approach allows study of the kinetics of domain nucleation and

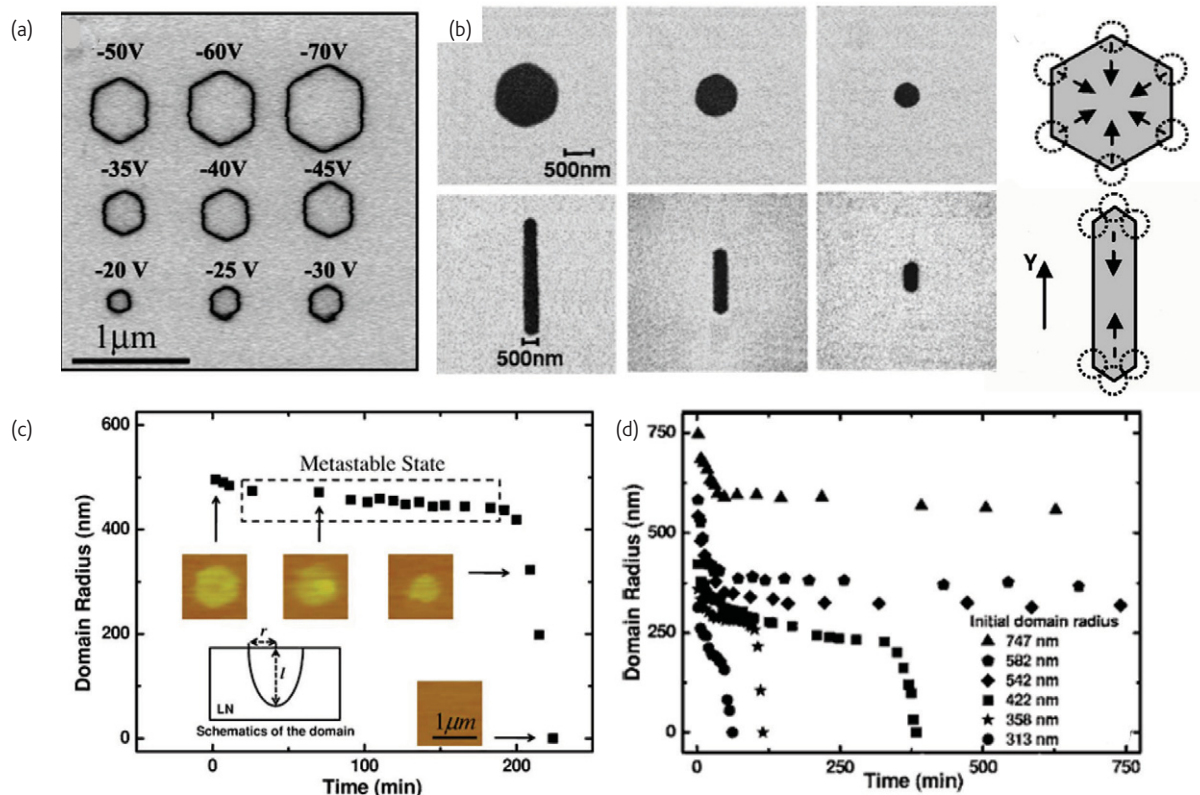


Fig. 3 Domain growth and relaxation by SPM. (a) Increasing domain radius in a lithium niobate single crystal with the magnitude of the applied voltage (reproduced with permission from Rodriguez et al.⁴⁵). (b) Thermal stability of fabricated domains (reproduced with permission from Liu et al.⁵⁵). (c, d) Stability of fabricated domain and dependence on initial domain size, respectively (reproduced with permission from Kan et al.⁴⁸).

subsequent growth at the tip-sample contact by control of the magnitude and duration of the applied field. The kinetics of domain growth⁴⁴⁻⁴⁸ have been studied in this fashion, primarily on single crystals. The radii of domains fabricated in lithium niobate single crystals (Fig. 3a) were found to scale linearly with applied field and approximately logarithmically with time. The time dependence of the domain wall velocity has been studied by several groups^{12,13,49,50}, who interpreted this as an exponential field dependence of wall velocity⁵¹. Recent studies of charge diffusion on the oxide surfaces and the role of humidity⁴⁵ on ferroelectric switching suggest that diffusion of charged species that minimize the depolarization energy of domains can mediate this kinetic behavior and lead to phenomena such as backswitching⁵² and formation of bubble-domains^{53,54}. Thus, domain growth in PFM is governed by the complex convolution of several factors, including thermodynamic effects such as field decay away from the probe and a decrease in total wall energy for large radii, and dynamic effects such as wall pinning and screening charge redistribution.

Complementary to domain growth are studies of relaxation behavior in the absence of an external field. These dynamics are driven by wall tension, and relaxation kinetics are determined by lattice, defect and surface pinning, thus offering greater potential for quantitative studies (albeit at the expense of long observation times). The thermal stability⁵⁵ and the retention behavior⁴⁶⁻⁴⁸ of fabricated domains have been studied in detail, as shown in Fig. 3b. In particular, the Kitamura group⁴⁷ has shown that for large domain sizes the relaxation dynamics are controlled by the regions of maximal

curvature (edges), as can be expected from simple thermodynamic considerations. Surface irradiation with high-energy ions introduces effective pinning sites and precludes domain relaxation. Finally, relaxation kinetics are very sensitive to the presence of surface adsorbates which are ubiquitous on ferroelectric surfaces exposed to atmosphere⁵⁶. A highly detailed study of domain relaxation as a function of domain size and crystal thickness was reported by Kan *et al.*⁴⁶ Data in Fig. 3c and d suggest an elegant two-step mechanism in which the slow relaxation stage involves lateral shrinking of the cylindrical domain, with subsequent pinch-off from the bottom surface, and fast relaxation of the resulting semielliptical domain.

Studies of local ferroelectric switching have attracted much effort due to applications to ferroelectric data storage³ and ferroelectric lithography⁵⁷⁻⁵⁹. In particular, recent results from Cho's group⁶⁰ demonstrate the formation of 2 nm domains, following his earlier demonstration of 8 nm domain arrays⁶¹. This impressive result corresponds to an information density of 160 Tb/inch² (10 Tb/inch² for the arrays), approaching the molecular storage density limit and clearly demonstrating the potential of ferroelectric materials for data storage. Extensive research on nanofabrication using ferroelectric lithography is now underway.

PFM spectroscopy and switching spectroscopy PFM

Understanding the effects of defects on polarization reversal requires the switching behavior to be probed at multiple points on a sample surface. The imaging approach described above provides only limited

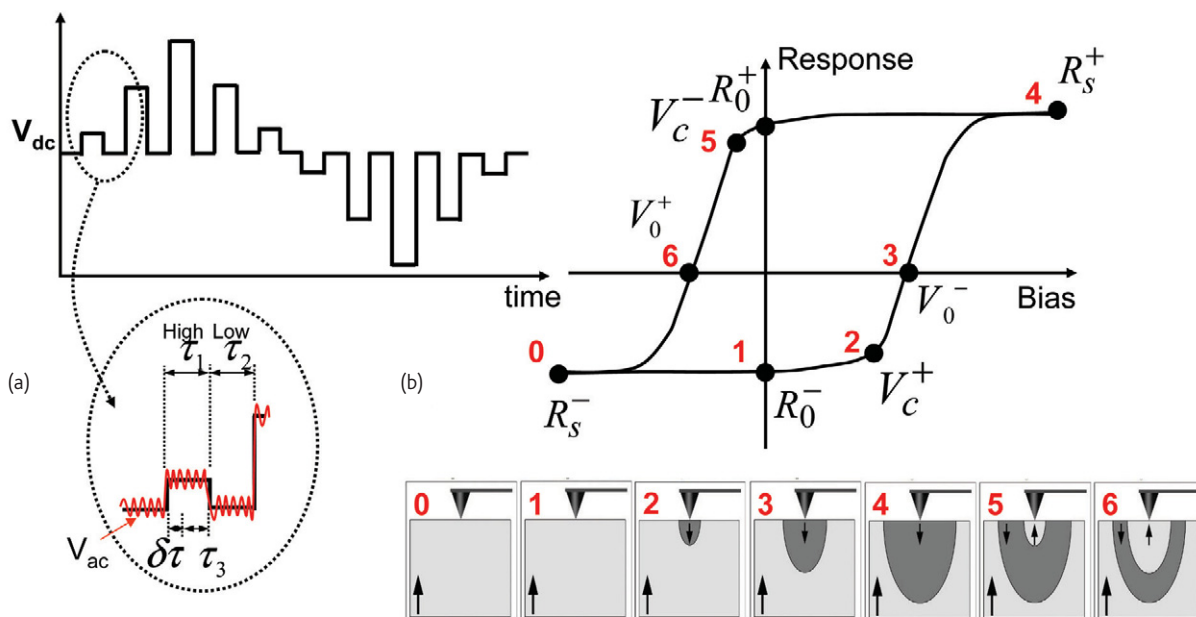


Fig. 4 Piezoresponse force spectroscopy. (a) Bias waveform for electromechanical spectroscopy measurements. (b) Model hysteresis loop with switching parameters labeled and corresponding domain nucleation progression. Both in-field and remanent piezoelectric hysteresis loops can be measured. Adapted with permission from Jesse *et al.*⁶⁵.

information on the spatial variability of switching behavior due to (a) time requirements ($\sim 1\text{--}10$ hours/location), and (b) the resolution limit, i.e. the smallest domains (corresponding to the as-nucleated state) can be below the resolution limit of the system. At the same time, capacitor-based studies address switching at all sites simultaneously, where the switching is initiated at the strongest sites (i.e. with the lowest nucleation bias) and subsequent domain growth overshadows the response of the weaker ones.

In Piezoresponse Force Spectroscopy (PFS), a sequence of voltage pulses is applied between the tip–sample contact and the bottom electrode to induce switching. At the same time, an AC voltage is applied to measure the local piezoresponse, as shown in Fig. 4. Domain nucleation and growth beneath the tip yields the characteristic piezoelectric hysteresis loop. The advantage of this approach is that a spectrum at a single point can be acquired in $\sim 0.1\text{--}1$ s, thus allowing for spatially resolved spectroscopic measurements. Note that direct information on the domain size is lost, necessitating development of deconvolution algorithms to establish the relationship

between measured PFM signal and size of the domain formed below the tip⁴³.

Examples of PFS hysteresis loops in comparison with macroscopic polarization–voltage loops for ferroelectric and antiferroelectric materials are shown in Fig. 5. The overall loop shape and evolution with bias are almost identical. Remarkably, even the widths of the loops are close (8 V for polarization–voltage, 12 V for PFM). This similarity is belied by the fact that the underpinning signal formation mechanisms are fundamentally different: the macroscopic loop is a result of a statistical process of nucleation, growth and interaction of multiple domains, whereas in PFM a single domain forms and grows deterministically below the tip.

PFS offers two opportunities for understanding local polarization dynamics: (a) quantitative studies of local mechanisms for polarization switching and (b) mapping the spatial variability of switching behavior. In high-quality epitaxial films, the spatial separation between extended defects such as dislocations can exceed 100 nm^{18, 62–64}, as compared to the $\sim 10\text{--}30$ nm size of the domain detectable by PFM. This

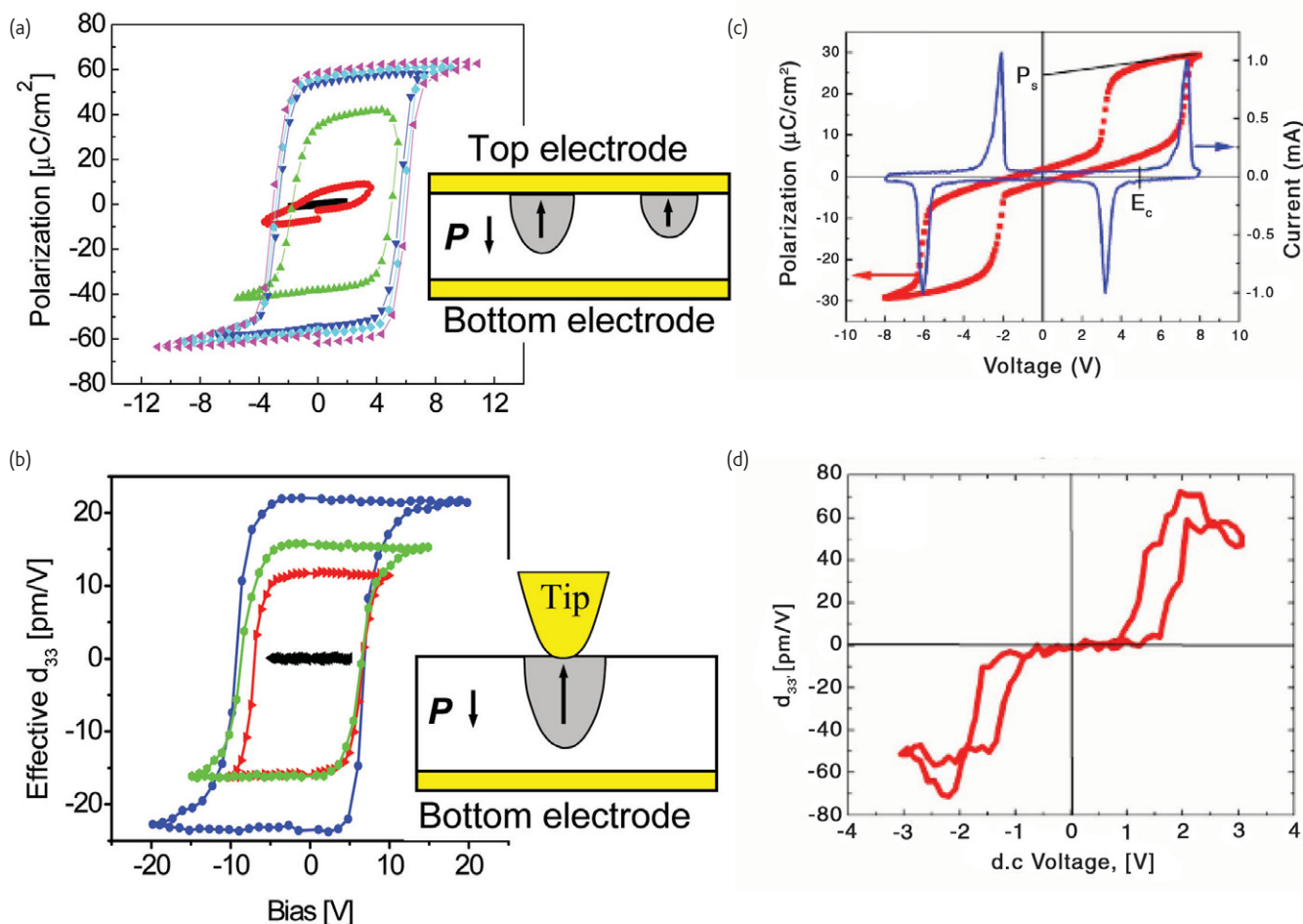


Fig. 5 Local vs. macroscopic measurements. (a) Polarization–voltage loops measured on a BiFeO_3 (BFO) capacitor (measurement schematic shown as inset). (b) Local hysteresis loops measured on a BFO film using the tip as a top electrode (inset). (c) Macroscopic and (d) local antiferroelectric to ferroelectric bias-induced transition in 001_{O} -oriented PZO film. (a,b) Adapted with permission from Kalinin et al.⁶⁷. (c,d) Reproduced with permission from Boldyreva et al.¹¹⁰.

comparison suggests that switching can potentially be studied on the level of a single defect.

The natural limitation in these measurements is that the positions of the defects are not known and can in only a few cases be determined from surface topography. Switching Spectroscopy PFM (SS-PFM) was developed to address this challenge⁶⁵. In SS-PFM, hysteresis curves are collected at each point in an image (Fig. 6a) and stored in a three-dimensional data array for subsequent examination and analysis. Phenomenological parameters describing the switching process, such as positive and negative coercive biases, imprint voltage, and saturation response, can be extracted from the data sets and plotted as two-dimensional maps of spatially resolved switching properties that can be correlated with PFM and surface topography⁶⁶.

While the full potential of SS-PFM has yet to be determined, this technique has already been used to study intrinsic polarization switching on a defect-free surface⁶⁷, ferroelectric properties in multiferroic structures⁶⁸, switching at bicrystal grain boundaries⁶⁹ and ferroelastic walls⁷⁰, to reconstruct the frozen Polarization layers in a lead Zirconate Titanate (PZT) nanoparticle⁷¹, and to map disorder potential components in epitaxial ferroelectric thin films⁷², as shown

in Fig. 6. The emergence of model materials systems with atomistically defined defects will allow polarization switching behavior to be linked to atomic structure.

The advances in SS-PFM have stimulated an extensive theoretical effort in understanding and quantitative description of piezoresponse spectroscopy. The detailed analysis of switching in bulk materials and thin films in the Landauer approximation for domain geometry was performed by Molotskii⁷³ and Emelyanov⁷⁴. Recently, Morozovska *et al.*^{38,41,43} have developed a quantitative pathway to analyze and interpret SS-PFM data in ferroelectric and antiferroelectric materials, including:

1. Calculation of the spatial distribution of the driving force for the phase transition for a known tip geometry.
2. Analysis of the energy parameters of the phase transition in a non-uniform field and establishment of the bias-dependent domain size in an ideal material and in the vicinity of defects.
3. Establishment of the relationship between the size of a phase-transformed region and the measured response for a known tip geometry.
4. Determination of the tip geometry using an appropriate calibration.

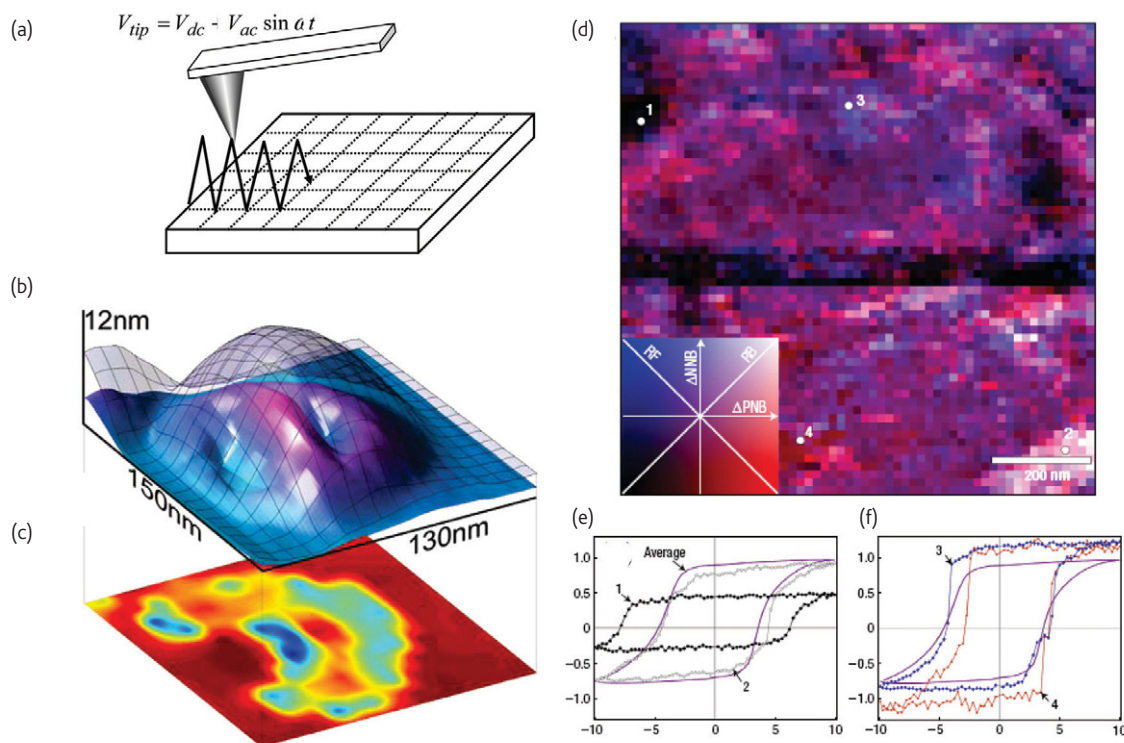


Fig. 6 (a) Schematic of tip movement during SS-PFM. (b) Topography (wire frame) and frozen-active layer interface (solid surface) of a PZT nanoparticle as determined from analysis of two-dimensional SS-PFM data (c) Map of the corresponding imprint bias for the switchable part of the nanoparticle. (d) Random-Field (RF) and Random-Bond (RB) disorder map for an epitaxial PZT film as determined from analysis of two-dimensional SS-PFM data. The axes on the color map are defined as the local deviations of the positive and negative nucleation biases from their global averages. The diagonals of the color map indicate correlations between changes in Positive and Negative Nucleation Bias (PNB and NNB), i.e. the relative degrees of random field and random bond. Example loops of random-bond (e) and random-field (f) disorder from locations indicated in (d). (b,c) Reproduced with permission from Rodriguez *et al.*⁷¹. (d)–(f) Reproduced with permission from Jesse *et al.*⁷².

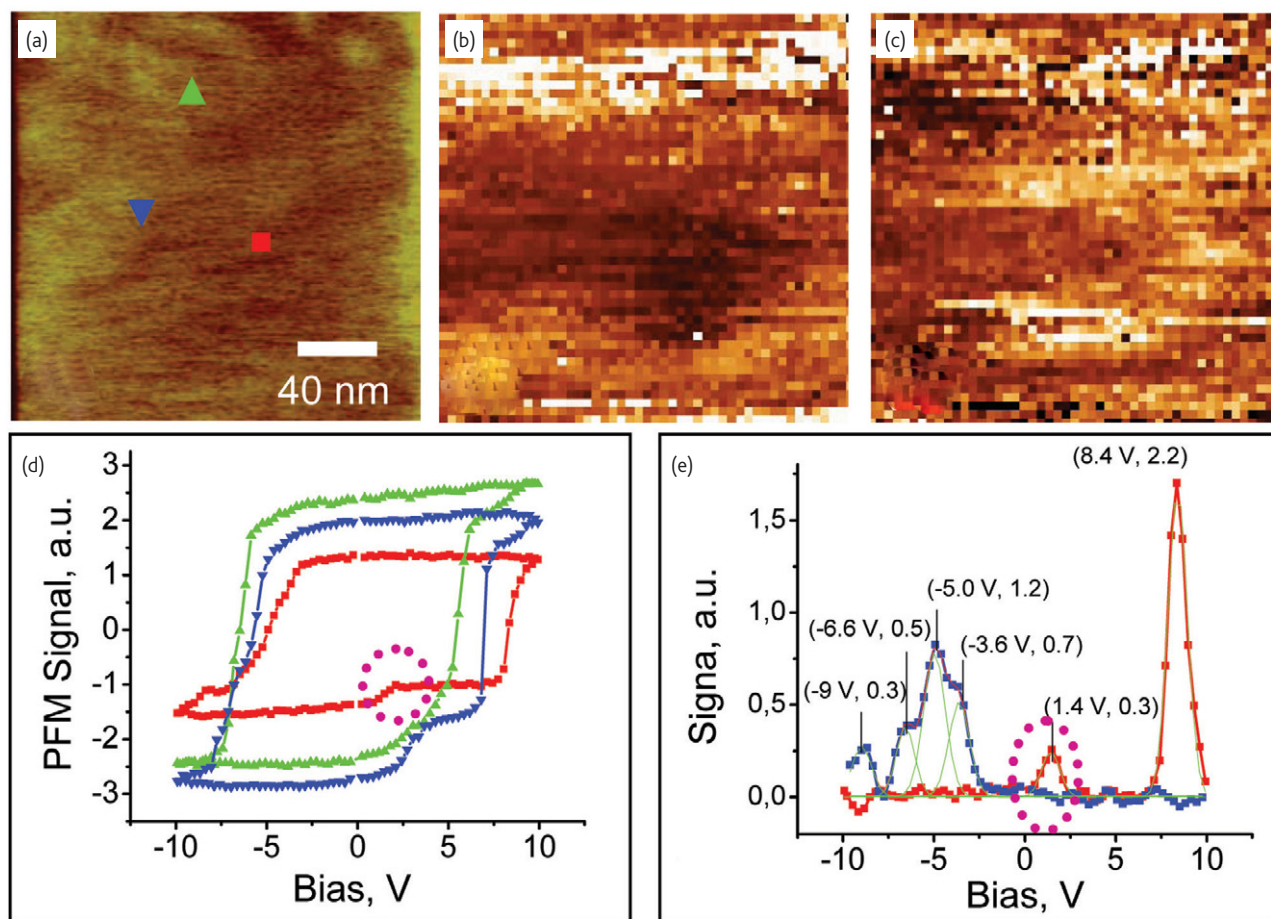


Fig. 7 Imaging single defect by SSPFM. (a) Topography, (b) nucleation bias map, and (c) fine structure intensity map. (d) Hysteresis loops from locations marked in (a), and (e) derivative of red loop in (a) revealing fine-structure in the hysteresis loop. Note the initial nucleation event circled in (d) and (e). Adapted with permission from Kalinin *et al.*⁸¹.

While most of the analytical efforts to date have been performed using the rigid ferroelectric approximation (infinitely thin domain walls) and semielliptical domain geometry, recent progress in PFM modeling by phase-field methods⁷⁵⁻⁷⁷ and analytical theory suggests that this approach can be significantly improved to include mesoscopic and atomistic effects.

The advances in PFM data acquisition have demonstrated that hysteresis loops often contain reproducible fine structure features, somewhat similar to structures in force–distance curves in atomic force microscopy. Studies by the Alexe group^{78,79} have associated the presence of fine structure features with proximity to a ferroelastic domain wall. Bdiin *et al.*⁸⁰ have performed simultaneous imaging and spectroscopic studies and illustrated that the fine structure is associated with nonmonotonic jumps in wall motion, i.e. individual pinning events. Finally, Kalinin *et al.*^{81,82} have predicted the signature of a single localized defect in SS-PFM nucleation bias and fine structure intensity images, and experimentally demonstrated the single-defect observation in epitaxial BiFeO₃ films (Fig. 7).

Other transitions

While studies of bias-induced polarization switching in ferroelectrics constitute the vast majority of PFM studies to date, the applicability of this technique extends well beyond this class of materials. As an example, local and macroscopic hysteresis loops in Fig. 5c and d illustrate spectroscopic evidence of a tip-induced local antiferroelectric-ferroelectric phase transition. In this case, no stable remanent state is observed at zero field. A second example is ferroelectric relaxors, in which the observed piezoresponse is strongly influenced by the mesoscopic disorder⁸³⁻⁸⁸. For relaxors, the random patterns of nanodomains reflect internal electric fields and stresses that destroy the long-range ferroelectric state. A statistical analysis of these nanodomains yields new information about the nature of defects responsible for disorder⁸⁸, grain boundary phenomena⁸⁹, and temperature evolution of the local order parameter^{16,88}. Hierarchical domain states on nano, meso, and macroscopic scales were simultaneously observed^{84,85}, leading to a better understanding of the giant piezoelectric effects in these materials. Mapping of the relaxation

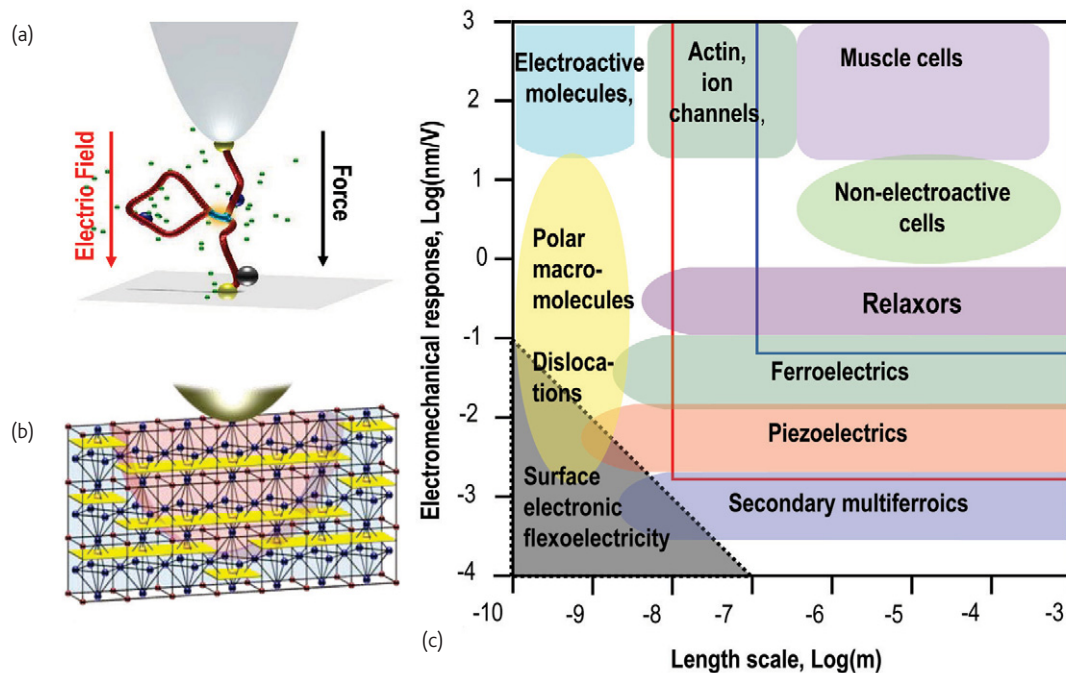


Fig. 8 Artistic vision of (a) bias-induced phase transitions in a molecule and (b) on a single-unit-cell level in a ferroelectric. (c) Electromechanical response roadmap depicting the relationship between length scale and system response. The blue and red lines correspond to areas accessible by nanoindentation and scanning probe microscopy, respectively.

parameters provides a better understanding of the nature of broad dielectric spectra in polycrystalline relaxors⁹⁰.

The original focus of PFM on ferroelectrics is due to (a) applications requirements, as well as (b) a readily interpretable contrast of domain

patterns and switchable polarization and (c) high electromechanical coefficients that make imaging and spectroscopy relatively straightforward. The development of low-noise detectors has allowed imaging and modification of biological materials^{91–93} that often possess

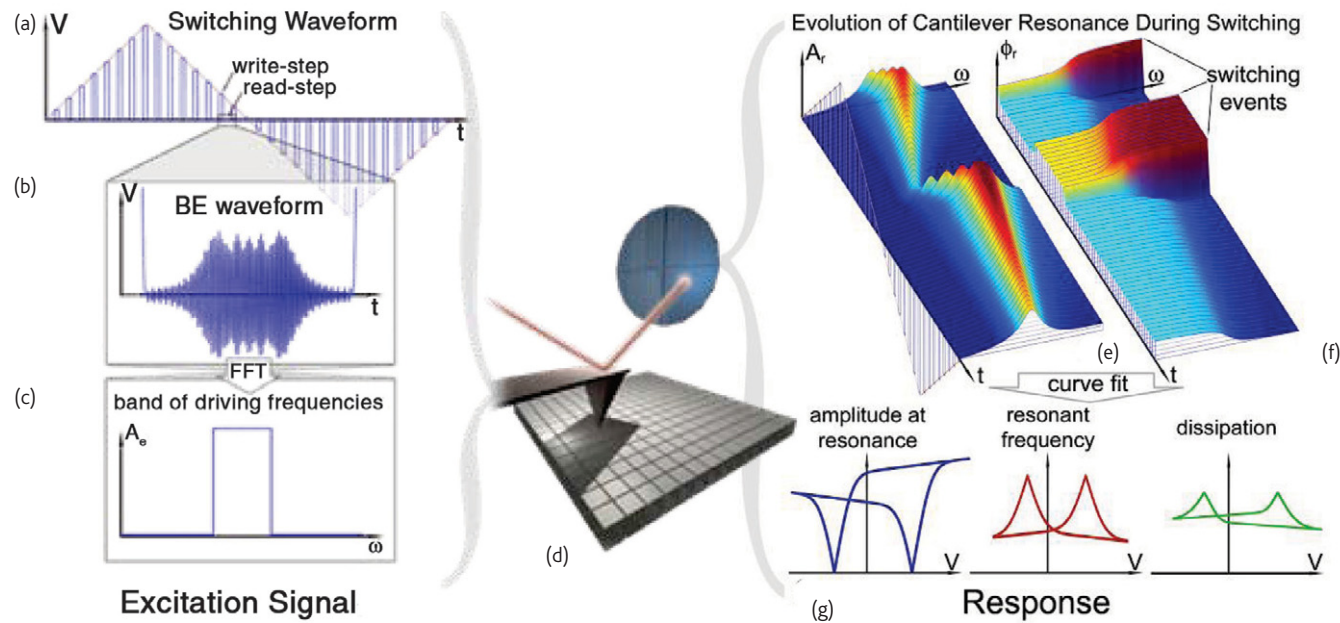


Fig. 9 Multidimensional modes of PFM. (a)–(c) Schematic depicting the use of a band of frequencies (band excitation) instead of a single-frequency modulation voltage during the application of a DC waveform to the tip (d) and during switching spectroscopy measurements. (e) The evolution of the cantilever resonance at switching events in (f). (g) Dynamic modes allow the resonance and the dissipation to be measured during hysteresis loop acquisition.

weak piezoelectric properties, typically $\sim 1\text{--}5$ pm/V, as compared to $10\text{--}500$ pm/V for ferroelectrics⁹⁴⁻⁹⁷. Electromechanical imaging and manipulation of biological systems necessitates performing PFM in a liquid environment⁹⁸. Studies using model ferroelectric systems have demonstrated that high-frequency PFM is feasible even in conductive liquids⁹⁹, while polarization switching and localization of the DC field¹⁰⁰ requires specially fabricated shielded probes¹⁰¹.

Challenges and opportunities

The PFM studies of polarization reversal in ferroelectric materials illustrate that bias-induced phase transformations can be studied with a single defect resolution. This progress naturally leads to a question of whether the same approach can be applied to mapping local electrochemical reactions in solids, probing shape changes during electrochemical transformation in macromolecules and force control of electrochemical reactions and ultimately probing the bias-induced transition on the level of a single unit cell.

The roadmap in Fig. 8 illustrates the sensitivity and length scales for electromechanical phenomena associated with bias-induced

transformations, as well as presents limits of PFM and piezoelectric nanoindentation measurements. Note that a broad spectrum of phenomena will become accessible with a 1–1.5 order of magnitude increase in resolution and $\sim 1\text{--}2$ order of magnitude increase in sensitivity, providing a clear perspective for technique development. The individual challenges on this pathway are (a) technique development to increase resolution, selectivity and sensitivity; (b) atomistic control of environment; (c) identifying appropriate material and defect systems; and (d) theory.

Progress in SPM detection has proceeded through the development of novel dynamic modes for resonance frequency tracking¹⁰²⁻¹⁰⁴, as well as small cantilevers and low-noise laser sources. An intrinsic requirement for PFM is decoupling between electrostatic and electromechanical interactions, a task that can be achieved only through precise engineering of tip size or tailoring the antiresonances of the cantilever response. The complexity of the problem and potential for this direction can be illustrated by a data acquisition in a four-dimensional multispectral band excitation SS-PFM shown in Fig. 9. This approach decouples the changes in electromechanical

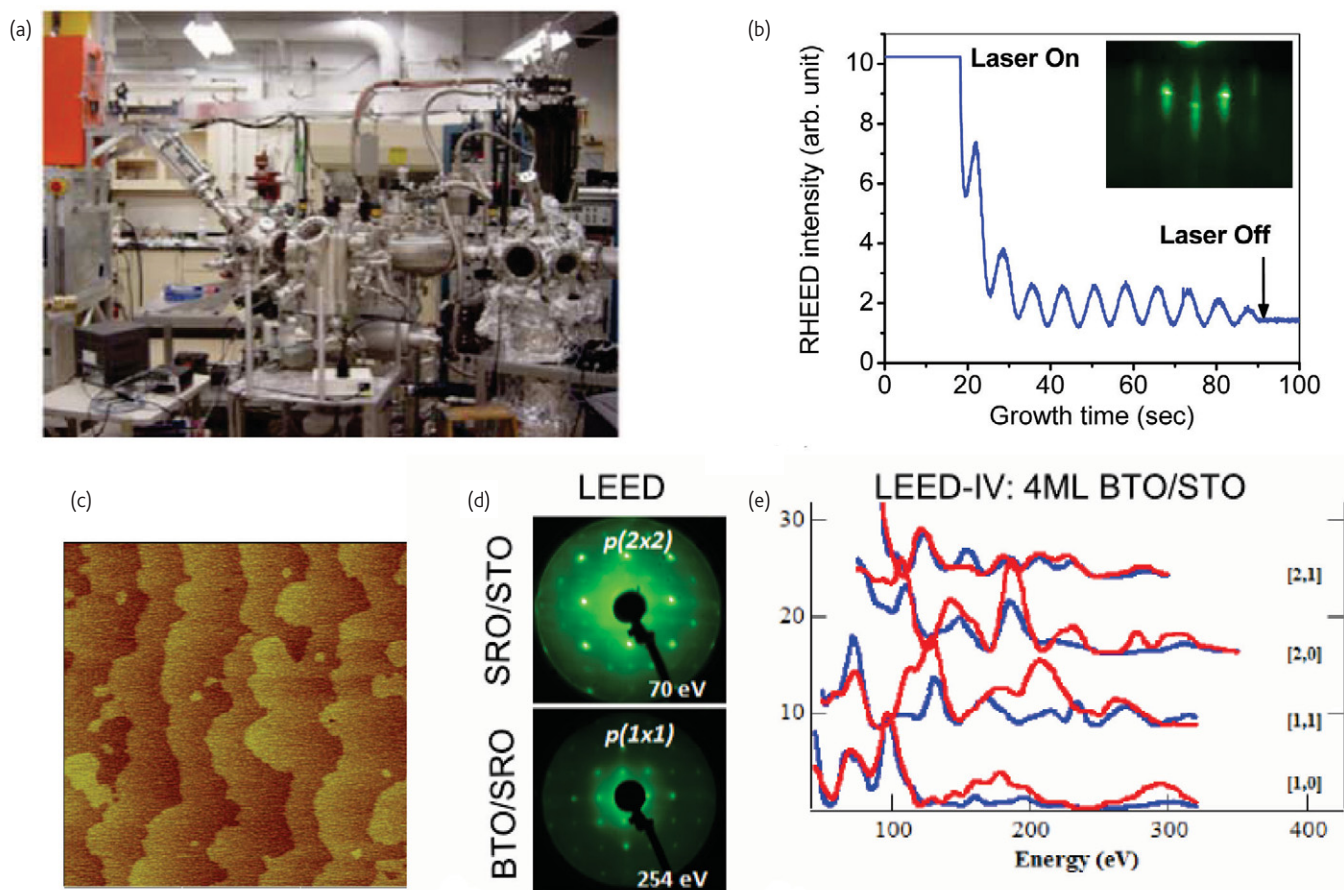


Fig. 10 (a) UltraHigh Vacuum (UHV) growth and characterization chamber for in-situ studies of oxide films. (b) Reflection High Energy Electron Diffraction (RHEED) intensity as a function of growth time illustrating potential for atomic-level control of growth. (c) Topography of in situ grown BaTiO_3 film. (d) Low Energy Electron Diffraction (LEED) patterns of SrRuO_3 and BaTiO_3 showing the surface reconstruction. (e) LEED intensity vs. voltage of $\text{BaTiO}_3/\text{SrRuO}_3/\text{SrTiO}_3$ film allows determination of the atomic structure of the first one or two monolayers.

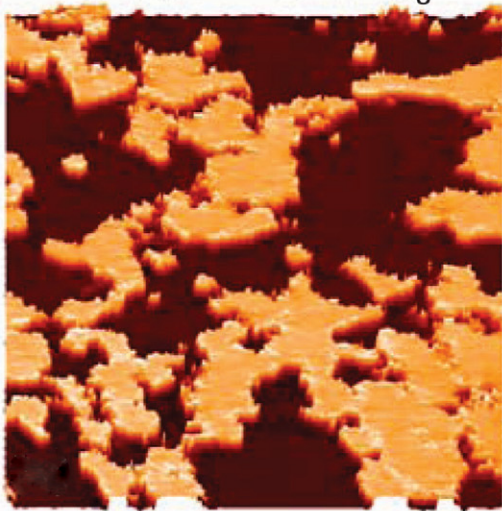
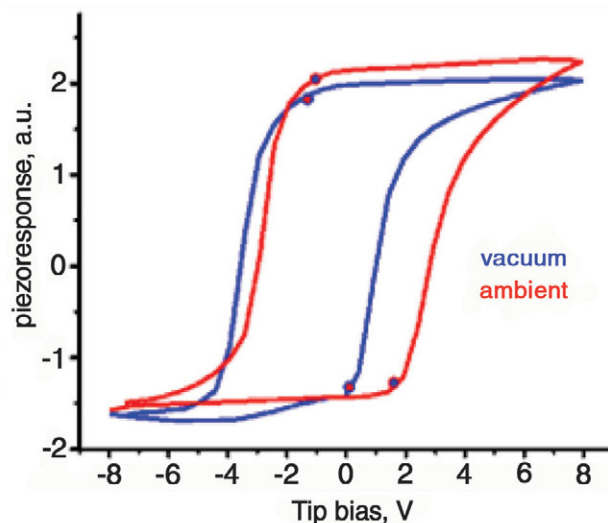
(a) UHV PFM: 5 nm BiFeO₃

 (b) Ambient vs UHV PFS: 200 nm BiFeO₃


Fig. 11 (a) UHV PFM of a *ex-situ* grown 5 nm BiFeO₃ thin film and (b) hysteresis loops measured from a 200 nm BiFeO₃ film in ambient and in UHV (sample courtesy of R. Ramesh, UC Berkeley).


response and local elastic properties and dissipation during local hysteresis loop measurements, providing a detailed insight into local wall motion¹⁰⁵.

All bias-induced phase transitions are sensitive to the presence of charged species, either directly (electrochemical reactions), or indirectly (e.g. screening and depolarization fields that control ferroelectric polarization switching). This necessitates atomistic control of the environment—either in an electrochemical liquid medium for fluid-mediated processes, or by studies of *ex situ* and *in situ* grown ferroelectric films, as illustrated in Figs. 10 and 11.

Understanding the atomistic mechanisms of switching requires properties to be studied to a level of a single (known) defect. This requires either materials with engineered defect structures such as bicrystal grain boundaries¹⁰⁶, threading dislocation or periodic dislocation arrays, or *in situ* PFM combined with structural techniques, such as electron microscopy¹⁰⁷. Finally, modeling and data interpretation tools for multidimensional data sets are clearly required to establish and understand the relationship between measured functionality and atomic structure.

Summary

PFM and its spectroscopic and dynamic offshoots have emerged as a powerful family of methods for probing dynamics of bias-induced

phase transitions in ferroelectrics. This progress has been possible because of PFM's ability to detect vertical and lateral contrast and the availability of a broad spectrum of spectroscopic modes. PFM's weak sensitivity to topographic cross-talk makes the measurements reproducible and quantitative even on nonatomically flat surfaces. The strong electromechanical coupling, readily interpretable domain contrast, and reversibility of phase transitions render ferroelectrics an ideal model for these studies and multiple advances in high-resolution imaging, including single-defect imaging, have been demonstrated. The future will undoubtedly see atomic-level studies on an engineered defect structure (including imaging in vacuum and in liquid), perhaps on a single unit cell level, and mapping of energy transformations in molecular systems. This will both lead to new advancements in areas such as information technology, data storage, energy technology, electrophysiology, as well as new serendipitous areas we can only imagine. 

Acknowledgments

Research at the Center for Nanophase Materials Sciences was supported by the Scientific User Facilities Division, Office of Basic Energy Sciences, US Department of Energy (S.V.K., B.J.R., S.J., P.M., K.S., and A.P.B.). One of the authors (B.J.R.) acknowledges the financial support of the Alexander von Humboldt Foundation. Thanks are also due to the Portuguese Foundation for Science and Technology (project PTDC/FIS/81442/2006) and to Scientec for the support within joint CICECO-Agilent PFM laboratory (A.K.).

REFERENCES

- 1 Waser, R. (ed.) *Nanoelectronics and Information Technology*, Wiley-VCH, Berlin, (2005)
- 2 Scott, J. F., *Ferroelectric Memories*, Springer, New York, (2000)
- 3 Tybell, T., *et al.*, *Appl. Phys. Lett.* (1999) **75**, 856

- 4 Pirovano, A., et al., *IEEE Trans. Electron. Dev.* (2004) **51**, 452
- 5 Miao, F., et al., *Phys. Rev. Lett.* (2008) **101**, 016802
- 6 Terabe, K., et al., *Nature* (2005) **433**, 47
- 7 Levanyuk, A. P., and Sigov, A.S., *Defects and Structural Phase Transitions*, Gordon and Breach, New York, (1987)
- 8 Ishibashi, Y., and Takagi, Y., *J. Phys. Soc. Jpn.* (1971) **31**, 506
- 9 Avrami, M., *J. Chem. Phys.* (1939) **7**, 1103
- 10 Kolmogorov, A. N., *Izv. Akad. Nauk USSR, Ser. Math.* (1937) **3**, 355
- 11 Nattermann, T., et al., *Phys. Rev. B* (1990) **42**, 8577
- 12 Tybell, T., et al., *Phys. Rev. Lett.* (2002) **89**, 097601
- 13 Paruch, P., et al., *Phys. Rev. Lett.* (2005) **94**, 197601
- 14 Catalan, G., et al., *Phys. Rev. Lett.* (2008) **100**, 027602
- 15 Shvartsman, V. V., and Kholkin, A. L., *J. Appl. Phys.* (2007) **101**, 064108
- 16 Likodimos, V., et al., *Phys. Rev. B* (2001) **63**, 064104
- 17 Likodimos, V., et al., *Phys. Rev. B* (2002) **66**, 024104
- 18 Grigoriev, A., et al., *Phys. Rev. Lett.* (2006) **96**, 187601
- 19 Gruverman, A., et al., *Appl. Phys. Lett.* (2005) **87**, 082902
- 20 Kim, D. J., et al., *Appl. Phys. Lett.* (2007) **91**, 132903
- 21 Balzar, D., et al., *Phys. Rev. B* (2004) **70**, 092103
- 22 Nagarajan, V., et al., *Appl. Phys. Lett.* (2005) **86**, 192910
- 23 Misirliglu, I. B., et al., *Appl. Phys. Lett.* (2006) **88**, 102906
- 24 Alpay, S. P., et al., *Appl. Phys. Lett.* (2004) **85**, 2044
- 25 Canedy, C. L., et al., *Appl. Phys. Lett.* (2000) **77**, 1695
- 26 Wang, R., et al., *Phys. Rev. Lett.* (1998) **80**, 2370
- 27 Emelyanov, A. Y., and Pertsev, N. A., *Phys. Rev. B* (2003) **68**, 214103
- 28 Chu, M. W., et al., *Phys. Rev. B* (2005) **72**, 174112
- 29 Shibata, N., et al., *Nature* (2004) **428**, 730
- 30 Duscher, G., et al., *Nat. Mater.* (2004) **3**, 621
- 31 McGibbon, M. M., et al., *Science* (1994) **266**, 102
- 32 Rief, M., et al., *Science* (1997) **276**, 1109
- 33 Kalinin, S. K., et al., *Phys. Rev. B* (2004) **70**, 184101
- 34 Karapetian, E., et al., *Philos. Mag.* (2005) **85**, 1017
- 35 Makagon, A., et al., *Phys. Rev. B* (2007) **76**, 064115
- 36 Felten, F., et al., *J. Appl. Phys.* (2004) **96**, 563
- 37 Scrymgeour, D. A., and Gopalan, V., *Phys. Rev. B* (2005) **72**, 024103
- 38 Morozovska, A. N., et al., *Phys. Rev. B* (2007) **75**, 174109
- 39 Kalinin, S.V., et al., *Appl. Phys. Lett.* (2006) **88**, 232904
- 40 Eliseev, E. A. et al., *J. Appl. Phys.* (2007) **102**, 014109
- 41 Morozovska, A. N., et al., *J. Appl. Phys.* (2007) **102**, 074105
- 42 Morozovska, A. N., et al., *Phys. Rev. B* (2007) **76**, 054123
- 43 Morozovska, A. N., et al., *J. Appl. Phys.* (2007) **102**, 114108
- 44 Terabe, K., et al., *Appl. Phys. Lett.* (2003) **82**, 433
- 45 Rodriguez, B. J., et al., *Appl. Phys. Lett.* (2005) **86**, 012906
- 46 Kan, Y., et al., *Appl. Phys. Lett.* (2006) **89**, 262907
- 47 Liu, X., et al., *Phys. Scr.* (2007) **T129**, 103
- 48 Kan, Y., et al., *Appl. Phys. Lett.* (2007) **91**, 132902
- 49 Gruverman, A., et al., *Annu. Rev. Mater. Sci.* (1998) **28**, 101
- 50 Pertsev, N. A., et al., *Nanotechnology* (2008) in print
- 51 Dahan, D., et al., *Appl. Phys. Lett.* (2006) **89**, 152902
- 52 Kholkin, A.L., et al., *Nanotechnology* (2007) **18**, 095502
- 53 Kim, Y., et al., *Appl. Phys. Lett.* (2007) **90**, 072910
- 54 Bühlmann, S., et al., *Phys. Rev. B* (2005) **72**, 214120
- 55 Liu, X., et al., *Appl. Phys. Lett.* (2006) **89**, 142906
- 56 Peter, F., et al., *Appl. Phys. Lett.* (2004) **85**, 2896
- 57 Kalinin, S. V., et al., *Nano Lett.* (2002) **2**, 589
- 58 Kalinin, S. V., et al., *Adv. Mat.* (2004) **16**, 795
- 59 Hanson, J. N., et al., *Nanotechnology* (2006) **17**, 4946
- 60 Tanaka, K., et al., *Jpn. J. Appl. Phys.* (2008) **47**, 3311
- 61 Cho, Y., et al., *Nanotechnology* (2006) **17**, S137
- 62 Sun, H. P., et al., *Appl. Phys. Lett.* (2004) **84**, 3298
- 63 Jia, C.-L., et al., *Nat. Mat.* (2008) **7**, 57
- 64 Vrejoiu, I., et al., *Philos. Mag.* (2006) **86**, 4477
- 65 Jesse, S., et al., *Appl. Phys. Lett.* (2006) **88**, 062908
- 66 Jesse, S., et al., *Rev. Sci. Instrum.* (2006) **77**, 073702
- 67 Kalinin, S. V., et al., *Proc. Natl. Acad. Sci. USA* (2007) **104**, 20204
- 68 Rodriguez, B. J., et al., *Nanotechnology* (2007) **18**, 405701
- 69 Rodriguez, B.J., et al., to be submitted
- 70 Balke, N., et al., to be submitted
- 71 Rodriguez, B. J., et al., *Adv. Mater.* (2008) **20**, 109
- 72 Jesse, S., et al., *Nat. Mater.* (2008) **7**, 209
- 73 Molotskii, M., and Winebrand, E., *Phys. Rev. B* (2005) **71**, 132103
- 74 Emelyanov, A. Y., *Phys. Rev. B* (2005) **71**, 132102
- 75 Li, Y. L., et al., *J. Appl. Phys.* (2005) **97**, 034112
- 76 Li, Y. L., et al., *Acta. Mater.* (2002) **50**, 395
- 77 Ahluwalia, R., and Cao, W., *J. Appl. Phys.* (2003) **93**, 537
- 78 Le Rhun, G., et al., *Appl. Phys. Lett.* (2007) **90**, 012908
- 79 Le Rhun, G., et al., *Nanotechnology* (2006) **17**, 3154
- 80 Bdikin, I. K., et al., *Appl. Phys. Lett.* (2008) **92**, 182909
- 81 Kalinin, S. V., et al., *Phys. Rev. Lett.* (2008) **100**, 155703
- 82 Morozovska, A. N., et al., *Phys. Rev. B* (2008) in print
- 83 Vakhrushev, S. B., et al., *AIP Conf. Proc.* (2003) **677**, 74
- 84 Bdikin, I. K., et al., *Appl. Phys. Lett.* (2003) **83**, 4232
- 85 Bai, F., et al., *Appl. Phys. Lett.* (2004) **85**, 2313
- 86 Shvartsman, V. V., and Kholkin, A. L., *Phys. Rev. B* (2004) **69**, 014102
- 87 Shvartsman, V. V., and Kleemann, W., *IEEE Trans. Ultrason. Ferroelectr. Freq. Control* (2006) **53**, 2275
- 88 Shvartsman, V. V., et al., *Phys. Rev. B* (2008) **77**, 054105
- 89 Kiselev, D.A., et al., *J. Phys. D: Appl. Phys.* (2007) **40**, 7109
- 90 Kholkin, A.L., et al., unpublished
- 91 Kalinin, S.V., et al., *Appl. Phys. Lett.* (2005) **87**, 053901
- 92 Rodriguez, B.J., et al., *J. Struct. Bio.* (2006) **153**, 151
- 93 Kalinin, S.V., et al., *Ultramicroscopy* (2006) **106**, 334
- 94 Fukada, E., and Yasuda, I., *J. Phys. Soc. Jpn.* (1957) **12**, 1158
- 95 Lang, S. B., *Nature* (1966) **212**, 704
- 96 Anderson, J. C., and Eriksson, C., *Nature* (1970) **227**, 491
- 97 Marino, A. A., and Gross, B. D., *Arch. Oral Biol.* (1989) **34**, 507
- 98 Kalinin, S. V., et al., *Nanotechnology* (2007) **18**, 424020
- 99 Rodriguez, B. J., et al., *Phys. Rev. Lett.* (2006) **96**, 237602
- 100 Rodriguez, B.J., et al., *Phys. Rev. Lett.* (2007) **98**, 247603
- 101 Rodriguez, B.J., et al., *Appl. Phys. Lett.* (2007) **91**, 093130
- 102 Rodriguez, B.J., et al., *Nanotechnology* (2007) **18**, 475504
- 103 Jesse, S., et al., *Nanotechnology* (2007) **18**, 435503
- 104 Kalinin, S.V., et al., *R&D Mag.* (2007) Oct., 34
- 105 Bühlmann, S. and Murali, P., *Adv. Mat.* (2008) in press
- 106 Rodriguez, B. J., et al., unpublished
- 107 <http://www.nanofactory.com/>
- 108 Lupascu D. C. and Rabe, U., *Phys. Rev. Lett.* (2002) **89**, 187601
- 109 Kalinin, S. V., et al., *Annu. Rev. Mat. Res.* (2007) **37**, 189
- 110 Boldyreva, K., et al., *J. Appl. Phys.* (2007) **102**, 044111